NeuroImage 221 (2020) 117204

Contents lists available at ScienceDirect

NeuroImage

journal homepage: www.elsevier.com/locate/neuroimage

Conduction delays in the visual pathways of progressive multiple sclerosis patients covary with brain structure

Shai Berman[a,$,*], Yael Backner[b,$], Ronnie Krupnik[a], Friedemann Paul[c,d], Panayiota Petrou[e], Dimitrios Karussis[e], Netta Levin[b,$], Aviv A. Mezer[a,$]

[a] Edmond and Lily Safra Center for Brain Sciences, The Hebrew University of Jerusalem, Jerusalem, Israel
[b] fMRI Unit, Neurology Department, Hadassah-Hebrew University Medical Center, Jerusalem, Israel
[c] NeuroCure Clinical Research Center, Charité-Universitätsmedizin Berlin, Corporate Member of Freie Universität Berlin, Humboldt-Universität zu Berlin, Berlin Institute of Health, Berlin, Germany
[d] Experimental and Clinical Research Center, Max Delbrueck Center for Molecular Medicine, Charité-Universitätsmedizin Berlin, Berlin, Germany
[e] The Multiple Sclerosis Center, Hadassah-Hebrew University Medical Center, Jerusalem, Israel

A B S T R A C T

In developed countries, multiple sclerosis (MS) is the leading cause of non-traumatic neurological disability in young adults. MS is a chronic demyelinating disease of the central nervous system, in which myelin is attacked, changing white matter structure and leaving lesions. The demyelination has a direct effect on white matter conductivity. This effect can be examined in the visual system, where damage is highly prevalent in MS, leading to substantial delays in conduction, commonly measured with visual evoked potentials (VEPs). The structural damage to the visual system in MS is often estimated with MRI measurements in the white matter. Recent developments in quantitative MRI (qMRI) provide improved sensitivity to myelin content and new structural methods allow better modeling of the axonal structure, leading researchers to link white matter microstructure to conduction properties of action potentials along fiber tracts. This study attempts to explain the variance in conduction latencies down the visual pathway using structural measurements of both the retina and the optic radiation (OR).

Forty-eight progressive MS patients, participants in a longitudinal stem-cell therapy clinical trial, were included in this study, three and six months post final treatment. Twenty-seven patients had no history of optic neuritis, and were the main focus of this study. All participants underwent conventional MRI scans, as well as diffusion MRI and qMRI sequences to account for white matter microstructure. Optical coherence tomography scans were also obtained, and peripapillary retinal nerve fiber layer (pRNFL) thickness and macular volume measurements were extracted. Finally, latencies of recorded VEPs were estimated.

Our results show that in non-optic neuritis progressive MS patients there is a relationship between the VEP latency and both retinal damage and OR lesion load. In addition, we find that qMRI values, sampled along the OR, are also correlated with VEP latency. Finally, we show that combining these parameters using PCA we can explain more than 40% of the inter-subject variance in VEP latency.

In conclusion, this study contributes to understanding the relationship between the structural properties and conduction in the visual system in disease. We focus on the visual system, where the conduction latencies can be estimated, but the conclusions could be generalized to other brain systems where the white matter structure can be measured. It also highlights the importance of having multiple parameters when assessing the clinical stages of MS patients, which could have major implications for future studies of other white matter diseases.

1. Introduction

Multiple Sclerosis (MS) is a chronic demyelinating disease of the central nervous system, in which myelin is attacked, forming lesions and changing white matter structure (Compston and Coles, 2008). The number or volume of lesions, called lesion load, is a useful measure of disease activity, though discrepancies between lesion load and the clinical state of the patient often exist (Backner and Levin, 2018). The damage often affects the primary function of white matter tissue in the brain - the conduction of electrical signals along white matter tracts (Halliday et al., 1973). These effects offer a unique opportunity to examine the connection between conduction and pathway connectivity in disease.

Involvement of the visual system is highly prevalent in MS. The visual system is of particular relevance for studying conductivity in the white matter due to its clearly defined pathway from eye to cortex and its accessibility to a variety of tools and tests. The most common MS symptom associated with the visual system is optic neuritis, the demyelination of the optic nerve. It is the presenting system in 20–30% of MS patients and the majority would be affected by it at some stage of their disease (Costello, 2016). However, many MS patients also exhibit damage to the posterior visual pathway, caused by lesions in the optic radiation (OR) (Galetta et al., 2015; Petzold et al., 2017). Furthermore, studies on non-lesion containing tissue, called normal-appearing white matter (NAWM), report early axonal pathology also outside inflammatory demyelinating lesions (Pawlitzki et al., 2017; Raz et al., 2015). Therefore, much interest has recently risen over the use of visual measures to further the understanding of the disease by use of this well-defined, contained system. Many studies have made use of a wide variety of vi-

* Corresponding author.
E-mail address: shai.berman@mail.huji.ac.il (S. Berman).
$ Equally contributing authors

https://doi.org/10.1016/j.neuroimage.2020.117204
Received 12 April 2020; Received in revised form 22 July 2020; Accepted 23 July 2020
Available online 1 August 2020

sual measures, from behavioral tests such as low-contrast letter acuity (LCLA) (Balcer et al., 2015) and motion perception (Raz et al., 2011), through imaging methods such as optical coherence tomography (OCT) (Frohman et al., 2006; Oberwahrenbrock et al., 2018; Oertel et al., 2019; Petzold et al., 2017; Talman et al., 2010) to the electrophysiological visual evoked potential (VEP) test (Toosy, Mason, & Miller, 2014) in an attempt to characterize and study MS through the visual system.

One of the most valuable tools for clinical diagnosis and monitoring of MS is magnetic resonance imaging (MRI) (Nitz and Reimer, 1999). MRI is sensitive to tissue properties and recent developments in quantitative MRI (qMRI) and in particular diffusion MRI (dMRI) provide measurements with improved sensitivity and specificity to white matter organization and microstructure (Alexander et al., 2011; Kuchling et al., 2018; Kuchling et al., 2017; Weiskopf et al., 2015). Various qMRI measurements have been found to be sensitive to myelin content, (Berman et al., 2018; Helms et al., 2008; Meyers et al., 2017; Sled and Pike, 2001; Stüber et al., 2014) and dMRI can be used to model axon configuration and even axon diameter (Assaf and Blumenfeld-Katzir, 2008; Basser and Jones, 2002; Basser et al., 2000; Kaden et al., 2016; Zhang et al., 2012). Combining these approaches, it is also possible to estimate the axon g-ratio, the ratio between the inner and outer diameter of the myelin (Stikov et al., 2012). These improvements in measurements have led researchers to try and link the white matter microstructure to properties of conduction of action potentials along white matter fiber tracts (Berman et al., 2019; Drakesmith et al., 2019; Takemura et al., 2020).

The relationship between the structure and function of the visual system in MS has been previously evaluated. Recently, Backner et al. studied patients diagnosed with progressive MS. They found that retinal thinning, estimated using retinal nerve fiber layer (RNFL) thickness obtained through OCT, was correlated with VEP latencies. This was true for patients without prior history of optic neuritis, but was not seen in patients with optic neuritis (Backner et al., 2019). Another work found that in relapsing-remitting MS (RRMS) patients without prior optic neuritis, VEP latencies are correlated with lesion load and diffusion parameters along the OR (Alshowaeir et al., 2014). Similar results were found in a pilot study in RRMS patients using ultra-high field MRI (Sinnecker et al., 2015). Various DTI indices have been related to VEP latencies, but recently it was suggested that the non-directional estimate of mean diffusivity may be the best option for reflecting tissue damage in chronic lesions (Klistorner et al., 2018). While each of these studies is informative in explaining the variance in the VEP latency, it is important to combine the various measurements to assess their contribution to the delay in VEP latency, and this was not done in progressive MS patients.

VEP latencies theoretically reflect retinal, thalamic, and cortical processing times, as well as conduction time along the visual white matter pathway. They have also been previously shown to be related to head size (Gregori et al., 2006). Therefore, in this work we tested how much of the variance in VEP latencies could be explained using structural measurement of the retina (RNFL thickness and macular volume) and the OR (qMRI and dMRI parameters, length and lesion load). In other words, using the visual pathway in MS patients to examine the relationship between white matter connectivity and conductivity. We hypothesized that using multiple sources of structural measurements may improve the understanding of the VEP delays.

2. Methods

2.1. Subjects

Forty-eight progressive MS patients were enrolled in a longitudinal mesenchymal stem cell therapy study (NCT02166021) at the Hadassah-Hebrew University Medical Center, from January 2015 to June 2018. Study protocol included nine visits over the duration of a year. This study encompasses the last two visits, approximately three and six months following final treatment administration. Inclusion criteria were, as reported in (Backner et al., 2019), the 2010 revised McDonald criteria for MS (Polman et al., 2011), ages 25–64, disease duration of at least 3 years, progressive forms of MS, EDSS score of 3.5–6.5, and failure to respond to the currently-available registered treatments. Exclusion criteria were treatment with cytotoxic or immunomodulatory medications in the 3 months prior to inclusion, significant diseases that may risk the patient or interfere with results, active infections, severe cognitive decline, as tested by the Brief International Cognitive Assessment for MS (BICAMS) (Langdon et al., 2012), and previous cellular treatment of any kind.

As the VEP latency of patients with prior optic neuritis is likely more affected by optic nerve lesions (Halliday et al., 1973), the main focus of this work is on the patients without prior optic neuritis (n = 27). Results for patients with prior optic neuritis (n = 21) are included in the supplementary materials.

This study was approved by the Hadassah-Hebrew University Medical Center Ethics Committee. All participants gave written informed consent.

2.2. Data acquisition and analysis

All electrophysiological and imaging measures were taken at two consecutive time points, approximately 3 months apart.

2.2.1. Functional properties of the visual system: visual evoked potentials latency

Standard full-field pattern reversal VEPs were recorded on a Bravo VEP device (Nicolet Biomedical) by a trained technician. Lateral electrodes were placed at O1 and O2 with a reference electrode placed at Fz and a ground electrode placed at the vertex. P1 (time-to-peak) latencies were extracted using at least two repetitions for each eye, with the reported values being an average of the two recordings.

2.2.2. Structure of the visual pathway

Peripapillary Retinal Nerve Fiber Layer (pRNFL) Thickness and Macular Volume

Peripapillary retinal nerve fiber layer (pRNFL) thickness was recorded by trained technicians using spectral-domain OCT (Spectralis, Heidelberg Engineering) with automatic real time (ART) function for image averaging. pRNFL was derived from standard ring scans around the optic nerve head. Macular volume was derived from custom macula scans (30° × 25°, 61 B-scans, ART: 13 frames). All scans underwent quality control according to the OSCAR-IB criteria (Schippling et al., 2015). Automatic segmentation results were checked for errors and corrected, if necessary, by an experienced observer blind to the subjects' condition. The pRNFL thickness was missing for 2 subjects with no history of ON. Therefore, unless stated otherwise, any analysis that involved the pRNFL thickness included 25 subjects, while other analyses included 27 subjects.

MRI acquisition:

All scans were performed on a 3T magnet (Siemens Skyra). Qualitative images, including T1-weighted (MPRAGE) and T2-weighted scans (SPC), were acquired at a resolution of 1 mm isotropic. For quantitative assessment of tissue properties, two types of scans were used: Diffusion weighted images were acquired with a diffusion-weighted spin-echo sEPI sequence with a resolution of 2 mm isotropic. The acquisition included 64 directions, with a diffusion weighting of b = 1000 mm^2s^{-1}. For T1 and water fraction mapping, 3D Spoiled gradient echo (FLASH) images were acquired with different flip angles (α = 4°, 10°, 20° and 30°), TE/TR = 2.85/14 ms. The scan resolution was 1.5 mm isotropic.

For calibration, we acquired an additional spin-echo inversion recovery scan with an echo-planar imaging read-out (SEIR-*epi*). This scan was done with a slab-inversion pulse and spatial-spectral fat suppression. For SEIR-*epi*, the TE/TR was 49/2920 ms. TIs were 100, 600, 1200, and 2400 ms. We used 2-mm in-plane resolution with a slice thickness of 3 mm. Both the flash and the SEIR-*epi* scans were performed using 2 × GRAPPA acceleration.

MRI analysis

Whole-brain T1 maps, together with bias correction maps of B1+ and B1-, were computed as described in (Mezer et al., 2016; Mezer et al., 2013). In short, unbiased T1 maps were calculated using the variable flip angles which were corrected for B1 excite inhomogeneity using the unbiased SEIR data (Barral et al., 2010). Next, the T1 maps were used to calculate unbiased proton density (PD) maps. To separate PD from receive-coil inhomogeneity, we assume smooth coil functions and use a biophysical regularization, which finds local linear relationships between 1/T1 and PD. This method was found to be effective and robust to noise (Mezer et al., 2016). The PD is normalized according to values in CSF-only voxels in the ventricles, to produce water-fraction (WF) maps. Maps of the lipid and macromolecular tissue volume (MTV) are then calculated as 1-WF. The analysis pipeline for producing unbiased T1 and MTV maps is an open-source MATLAB code (available at https://github.com/mezera/mrQ).

Diffusion analysis and preprocessing included the following steps: Subjects' motion was corrected using a rigid body alignment algorithm. Diffusion gradients were adjusted to account for the rotation applied to the measurements during motion correction. The twice refocused spin echo sequence we used does not require eddy current correction (Reese et al., 2003). Preprocessing steps were implemented in MATLAB (MathWorks, Natwick, MI, USA) and are publicly available as part of the vistasoft git repository (see dtiInit.m). The preprocessed diffusion data were then fitted with a tensor model (Basser and Jones, 2002) from which the mean diffusivity (MD),the radial diffusivity (RD), and fractional anisotropy (FA) were calculated.

The optic radiations were delineated using the probabilistic fiber-tracking algorithm, ConTrack, to identify the most likely pathway between two ROIs (Sherbondy et al., 2008). The LGN and calcarine sulcus were manually and anatomically defined on the T1 maps of each participant. The LGN definition was also assisted by the extracted DTI RGB map of each participant. A collection of 75,000 possible pathways was sampled and the most likely optic radiations were estimated as those pathways scoring at the top 20% (15,000). Each fiber bundle was manually checked and cleaned of spurious fibers using the QUENCH tool (VISTA Lab, Stanford University). Fibers were considered spurious if they crossed to the contralateral hemispheres or if their trajectory greatly deviated from the tract core. Most discarded streamlines were either too superior or curved too anteriorly around Meyer's loop. Supplementary figure 1 shows the optic radiations of 5 randomly selected subjects. The figure shows some variability exists in the reconstruction of the OR, particularly in Meyer' s loop (which is only partially reconstructed in subjects 2, 4 and 5 from the left). We visually inspected the loops and graded them as fully, partially or not reconstructed. These categories were later used for assessing the effect of the reconstruction on the inter-subject variability. For a description of the reconstruction of the optic tract, and a discussion on its related results, see the supplementary material.

Lesions were automatically segmented based on T1-weighted and T2-weighted images. The algorithm, a classifier trained to detect white matter hyperintensities (Dadar et al., 2017), produced probabilistic maps and a threshold for creating lesion masks was chosen based on visual inspection. Manual correction was performed in areas with large errors in the lesion segmentation.

Metric computation

To estimate lesion load, we took several approaches. We first calculated the general lesion load by taking the volume fraction of lesions, divided by the volume of the white matter tissue (including lesions). We similarly calculated OR lesion load by taking the volume of lesioned area coinciding with the area of the OR, divided by the overall volume of the OR. Finally, we sampled the lesion mask along the core of the OR tracts, while weighting the lesions based on distance from the tract core (Yeatman et al., 2012; Schurr et al., 2018). This provides a tract profile that at each point ranges from 0 to 1, reflecting how much of the tract coincides with a lesion, and giving more weight to the tract core. Using the tract core to qMRI measurement allows for a more robust estimation of OR properties, that is less affected by the variance in the reconstructed tract. Averaging the tract lesion profile provides an estimate of the fraction of the tract that is damaged due to lesion.

The T1 maps (acquired with a non-*epi* readout) were registered to the diffusion space (acquired with an *epi* readout) using non-linear registration, with the ANTs software (Avants et al., 2009). To evaluate the parametric maps along the OR, the maps (MD, RD, FA, MTV and T1) were sampled along the tract in the same way that the lesion masks were sampled. Supplementary figure 2 shows the tract profiles of all subjects for T1, MD and the lesion load. This provides, for each OR, a tract profile of each parameter over 100 nodes (Yeatman et al., 2012). We took three approaches for summarizing the tract profile of the qMRI parameters. We average the values either over the entire tract, or over the nodes considered to be NAWM, or over nodes considered as passing through lesions (a node is considered to be NAWM if the lesion tract profile is smaller than 0.05). In all methods we only consider nodes 10–90, to avoid partial volume effects with the cortex and areas with high dispersion. To test whether the individual variability in the reconstruction of Meyer's loop might affect our results, we also calculated OR estimates while excluding the segment containing Meyer's loop. To do this we considered nodes 35–90 (we visually verified this indeed excludes Meyer's loop in all ORs). Finally, we also calculated the length of the OR fiber tract using its core.

2.2.3. Statistical analysis

To relate structural measurements to function, we set out to test how much of the variance in the VEP latency can be explained using the pRNFL and the OR structure, as measured with MRI. We used leave-one-out cross-validation approach, where a general linear model was fit using all data except a single point, and the prediction is calculated for the remaining data points. The model accuracy was assessed using the coefficient of determination (COD, R^2), and the mean absolute error between the measured and the predicted VEP latency.

To combine the different parameters while avoiding overfitting, we used principal component analysis (PCA) on the structural properties i.e. the pRNFL thickness, OR length, lesion load along the OR, and MD or T1 along the OR. The PCA was calculated on z-scored values, since standardizing the values maintains the inter-subject variance within measurement, while controlling for the difference in amplitudes between measurement. As a result, the contribution of each measurement to each PC is at the same scale and therefore can be compared. The projection of the subjects on the first PC was then used to predict the variance in the VEP latency.

To maximize the data size, we averaged the two final visits, which were 3 and 6 months post-treatment, respectively. Supplementary figure 3 shows the correspondence between the measurements in the 2 visits to show their average is indeed representative of the data. We used cross-validation to predict the VEP latency of one visit, given the other. The variance explained with this approach provides a ceiling on the variance we expect to explain using the structure measurements. Second, since the OR axons in a single hemisphere convey information originating from both eyes, we average both over the left and right OR data (for. MD, FA, MTV, T1 and lesion load), as well as over the left and right eyes (for pRNFL, and VEP latency). The correspondence between the left and right values can be seen in Supplementary figure 4. As expected from any repeated measurement, the values between the two final visits, and between the two sides, are not identical, nevertheless, there is no bias

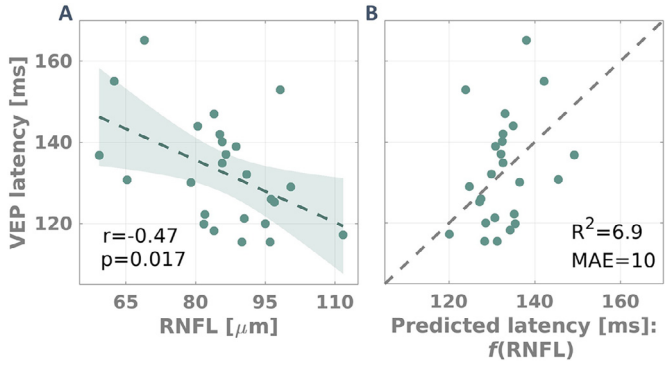

Fig. 1. Retinal thinning is related to VEP latency. A. VEP is negatively correlated with pRNFL thickness in subjects with progressive MS (r = -0.47). B. Leave one out cross-validation was used with a linear fit of pRNFL to create predictions of VEP latency. The mean absolute error (MAE) is around 10 ms, and the coefficient of determination (COD, R^2) between the measured and predicted latency is 7. (For interpretation of the references to colour in this figure legend, the reader is referred to the web version of this article.)

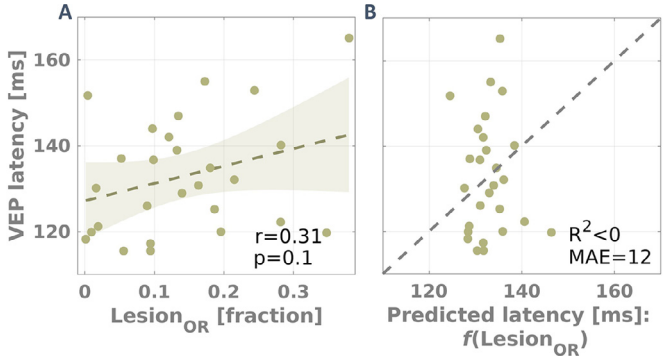

Fig. 2. OR lesion load and VEP latency. The lesion load along the OR was calculated as the average lesion tract profile, thus reflecting the relative overlap between the OR and the lesions, giving greater weight to the tract core. A. VEP latency is positively correlated (r = 0.31) with the lesion load of the OR (Lesion$_{OR}$). B. Cross-validation found Lesion$_{OR}$ alone is not sufficient to accurately predict the VEP latency. Other approaches for estimating the lesion load were evaluated and can be seen in supplementary figure 4. (For interpretation of the references to colour in this figure legend, the reader is referred to the web version of this article.)

or systematic differences between the values and they are very similar to one another.

2.2.4. Data availability

The data supporting the findings of this study are available from the corresponding author upon request.

3. Results

3.1. OCT

In our analysis we find that the relationship between pRNFL thickness and VEP latency, reported in (Backner et al., 2019) on the same cohort, pre-treatment, also persists post-treatment (r=-0.47) (Fig. 1). The pRNFL thickness accounted for about 7% of the variance in the VEP latency. Similar to the results in Backner et al., the macular volume was not significantly correlated with the VEP latency (r=-0.26, p = 0.29), and was not informative in predicting the VEP latency using cross-validation (R^2<0, MAE=12).

3.2. Lesions

Fig. 2a shows the correlation between the VEP latency and the OR lesion load, calculated as the average lesion tract profile (r = 0.31). Using cross-validation, we found it was not informative in predicting the VEP latency when used alone (Fig. 2b). To assure this result is not dependent on the way the lesion load was calculated, we also tested two alternative approaches for lesion load computation. We find the results to be similar in all three methods, and their comparison is presented in supplementary figure 5.

3.3. OR length

To test whether the VEP latency variance can be explained by the distance the signal has to travel, we calculated the length of the OR core tract profile. The OR length was not significantly correlated with the VEP latency (Fig. 3a), and cross-validation revealed it could not explain its variance (Fig. 3b). The figure clearly shows a single data point that is an outlier to the relationship, likely due to this subject's large lesion load which created a delay in its VEP peak time. Removing it increases the correlation (Fig. 3c).

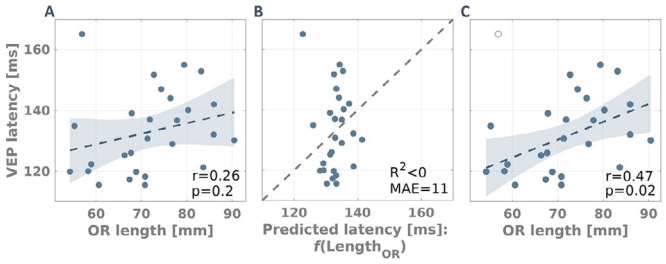

Fig. 3. OR length and VEP latency. The OR length is calculated using tract core. A. The VEP latency is not significantly correlated (r = 0.26, p = 0.2) with the OR tract length (Length$_{OR}$). B. Cross-validation found Length$_{OR}$ alone is not sufficient to accurately predict the VEP latency. C. The correlation increases (r = 047) when removing a subject that strongly deviated from the linear relationship between the VEP latency and the OR length (marked as an empty circle). (For interpretation of the references to colour in this figure legend, the reader is referred to the web version of this article.)

3.4. qMRI

Next, we tested the ability to predict the VEP latency using the quantitative parametric values that are sensitive to both changes in tissue microstructure and to lesions along the OR core. The MD values were found to be correlated with VEP latency (r = 0.59) (Fig. 4a). Quantitative T1 values also have a positive correlation with VEP latency (r = 0.56) (Fig. 4b). Using cross-validation (Fig. 4c-e) we found that the MD values lead to a similar prediction error as the T1 values (~10 ms), but do a better job explaining the between-subject variance as calculated with the COD (R^2=23 for MD, and R^2=17 for T1). Unlike MD and T1, the FA and MTV along the OR were not significantly correlated with the VEP latency (supp. Fig. 6ab), and therefore were not used in following analyses. We found the RD was highly correlated with the MD (r = 0.99), and consequently, it was also positively correlated with the VEP latency (r = 0.56, p = 0.03) (supp. Fig. 6c). Using cross validation revealed a slight disadvantage to RD (R^2 = 19) compared with MD. Given these results, and the non-directional nature of the MD, we will only consider MD in following analyses using dMRI.

Finally, we found that using both T1 and MD in the linear model does not increase the ability to explain variance of the VEP latency (R^2 = 17). This is probably due to overfitting, since the MD and T1 covary in the OR (supp. Fig. 7). Supplementary figure 8 shows that averaging MD and T1 only across NAWM nodes, or only across nodes that pass-through le-

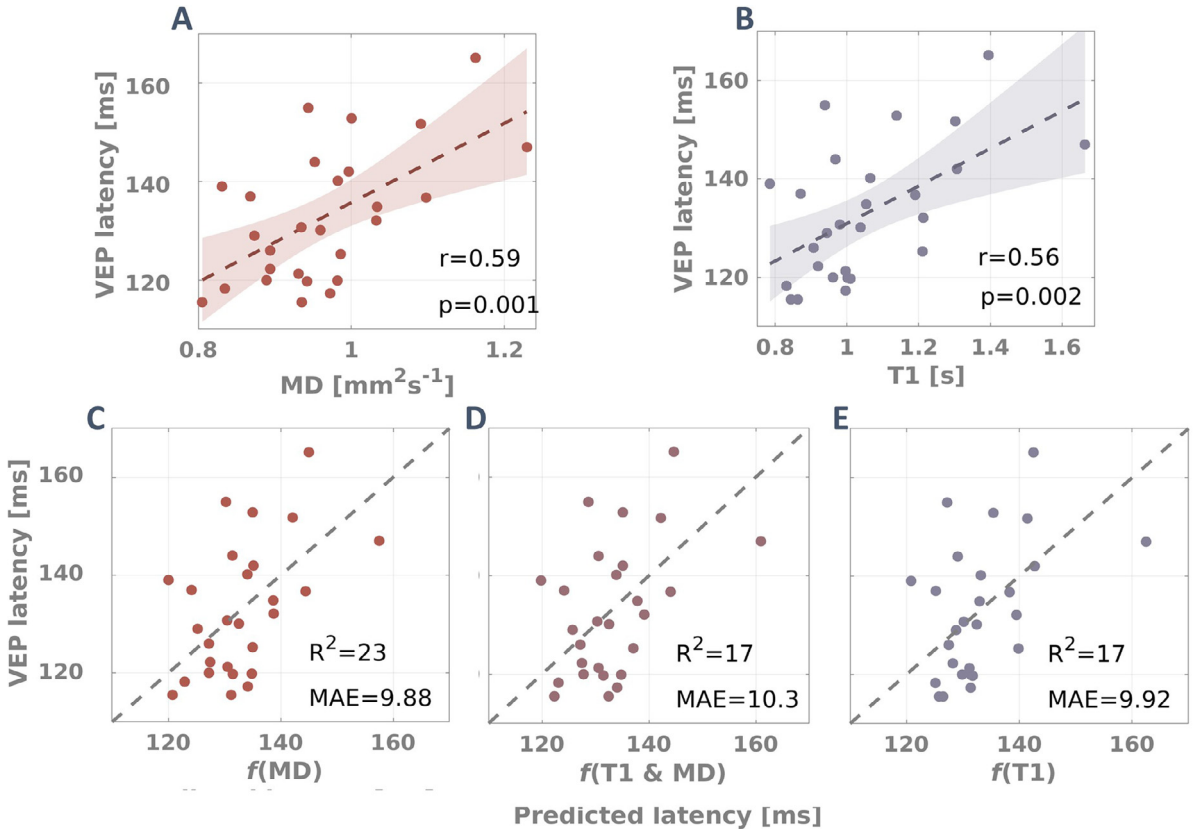

Fig. 4. QMRI along the OR is related to VEP latency. T1 and MD were sampled along the OR, and their average along the tract profile was calculated. The average of MD (A) and T1 (B) values along the OR are positively correlated with the VEP latency. Leave-one-out cross-validation found that T1 (E) underperforms MD (C) in predicting the VEP latency (R^2=17,23 respectively). Using both T1 and MD together (D) does not improve the prediction (R^2=17). Other approaches for estimating T1 and MD and their relationship with the VEP latency, as well as their relationship to one another can be seen in supplementary figures 7-8.

sions, is less successful in predicting the VEP latency compared to using the average across the entire tract. Finally, no correlation was found between qMRI values of the optic tract and VEP latencies. These results are discussed in the supplementary material (supp. Fig. 9).

3.5. Multi-parametric prediction of the VEPs

Finally, we tested whether it is beneficial to combine the different parameters. For this purpose, we calculated a PCA over the subjects' four structural variables that come from different sources: OR lesion load, OR length, pRFNL thickness and either T1 or MD, representing the OR microstructure. Fig. 5a shows the coefficients of each variable to the 1st principal component (PC). The 1st PC explains 37% or 39% of the structural variance when computed with T1 or MD, respectively. In either case the OR length contributes minimally to the 1st PC. The projection of the subjects on the 1st PC is highly correlated with the VEP latency, both when using T1 (Fig 5b), and when using MD (Fig. 5e). Using cross-validated prediction of VEP latency based on the 1st PC we can explain more than 45% of the variance in the VEP latency, with a slight advantage to using T1 in the PCA (Fig. 5c., R^2=49, MAE = 7.7), rather than MD (Fig. 5f., R^2 = 46, MAE = 8.1). The 2nd PC, which explain 25% of the structural variance, is not significantly correlated with the VEP latency and does not explain its variance. When using both T1 and MD in the PCA, the 1st PC explains more of the structural variance (46%, since T1 and MD are correlated), yet the correlation with the VEP latency is reduced (r = 0.69, cross-validation R^2 = 0.37).

Supplementary figure 10 shows the prediction given pairs of predictors. To allow for a fair comparison, we use the 25 subjects that have pRNFL thickness estimates for this pair-wise prediction of VEP latency. The combination of the OR lesion load either with MD values in the OR (supp. Fig. 10a.) or with pRNFL thickness (supp. Fig. 10c) allows to explain about 30% of variance in VEP latency, with similar prediction error (MAE = 8.9). Combining the MD values with the pRNFL thickness (supp. Fig. 9b) is slightly worse than simply using MD on its own.

To test whether the individual variability in the reconstruction of Meyer's loop is contributing to our results, we also calculated OR estimates while excluding the segment containing Meyer's loop. Supplementary figure 11 shows that the T1 and MD estimates are similar whether calculated across the entire OR tract or only across the section excluding Meyer's loop. Whatever differences are found, do not depend on the extent to which the Meyer's loop was reconstructed (supp. Fig. 11C,D). Furthermore, repeating the PCA analysis with the estimates excluding Meyer's loop reveal very similar results (cross-validation R^2 = 47, 53, when using T1, or MD, respectively).

3.6. Optic neuritis patient results

The same analyses, performed on the patients with reported history of unilateral optic neuritis (N = 16), failed to show a similar relationship between properties of the OR and VEP latencies. The data is presented in the supplementary materials (supp. Fig. 12).

4. Discussion

In this study we use the structure of the visual system, i.e. its connectivity and microstructure, to explain the variance in its VEP latency, i.e. conductivity. We find that for subjects with progressive MS (with no history of ON), pRNFL thickness and structural properties of the OR were correlated with the VEP latency, and when combined together they can explain more than 45% of the inter-subject variance. Specifically,

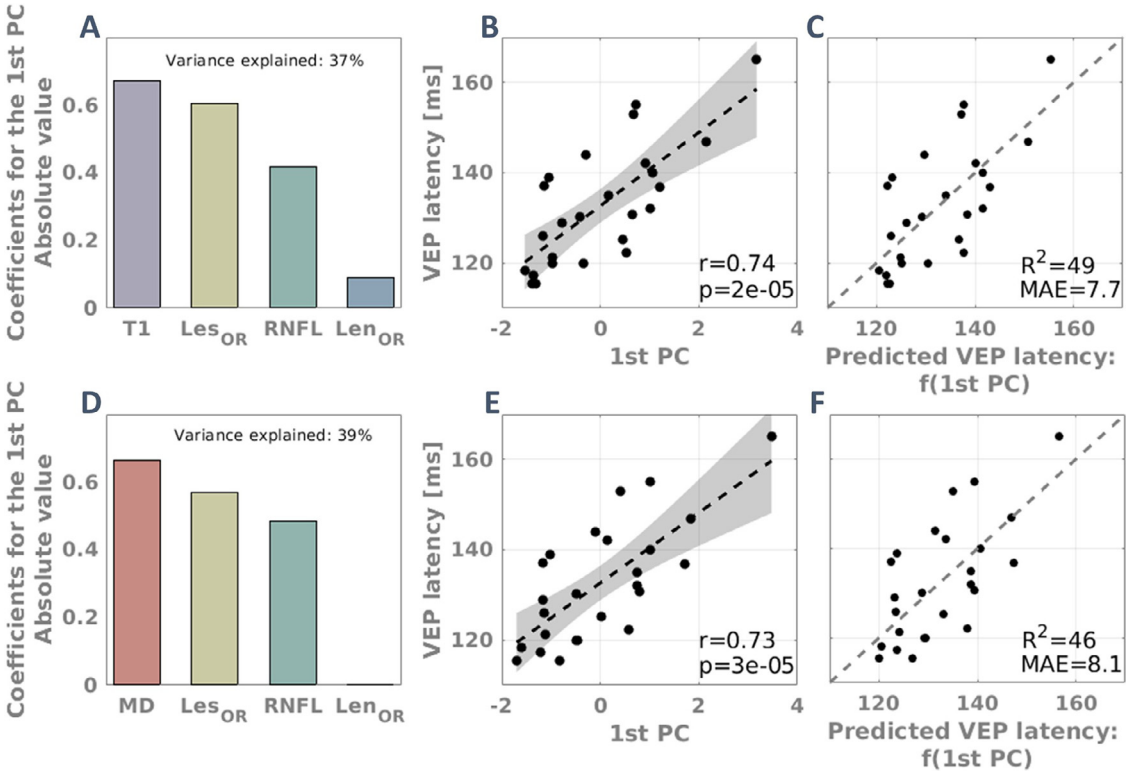

Fig. 5. PCA on the visual pathway structure. PCA was performed on the structural parameters, once with T1 as the measure of OR microstructure (top row), and once with MD (bottom row). The first principal component explains almost 37% of the inter-subject variance in the structure of the visual system using T1 (A) and 39% using MD (D). In both cases, the OR length contributes very little to the 1st PC. The projection of the subjects on the first PC is (B,E) correlated with the VEP latency ($r = 0.74$ with T1, $r = 0.73$ with MD, $p<10^{-4}$), and (C,F) using cross-validation the 1st PC explains more than 45% of the inter-subject variance in VEP latency, with T1 (MAE = 7.7) giving slightly better results than MD (MAE = 8.1). Using both of them (not shown) damages the prediction (MAE = 9). (For interpretation of the references to colour in this figure legend, the reader is referred to the web version of this article.)

using the 1st PC of the measures that reflect retinal thinning, the damage to the OR, and the OR microstructure we are able to predict the VEP latency - the extent to which the visual signal is delayed, with a mean absolute error of about 8 milliseconds. The contribution of each structural aspect can be seen both in the coefficients to the 1st PC, and in the separate analyses.

The visual system, being clearly defined and both structurally and functionally accessible, makes it possible to try and define the relationship between conductivity of the signal down the visual pathways and pathway connectivity. Electrophysiological studies that make use of the visual system in patients with MS usually examine patients with a history of optic neuritis, as VEP is a tool commonly used in its diagnosis. In these patients, a longer time-to-peak (P100) was found to be correlated with functional effects of the damaged nerve (Raz et al., 2011; Sanders et al., 1987). Delayed peaks in their fellow eyes were suggested to result from a wider VEP waveform to enable synchronization of the input between the eyes (Raz et al., 2013). In the current study in which we wished to refine the connection between conduction and connectivity, we separated patients with prior optic neuritis to avoid these possible interfering factors of functionality and adaptation.

The relationship between OR lesion load and VEP latency, has been previously shown for the non-optic neuritis eyes of RRMS patients (Alshowaeir et al., 2014). For the same patient group, it was also shown that neuronal loss (measured by pRNFL and ganglion cell layer thickness) is inversely correlated with the VEP latency (Sriram et al., 2014) and with lesion damage in the OR (Sinnecker et al., 2015), possibly through retrograde transsynaptic degeneration (Klistorner et al., 2014). More recently, Backner et al. (Backner et al., 2019) found that in the participants of the current study, prior to treatment, the pRNFL thickness is negatively correlated with the VEP latency. While pRNFL thickness and lesion load are correlated to one another, we found that combining these two parameters together increases the explained variance in VEP latency. These results suggest that while the retinal thinning and OR damage may be related to each other, they seem to represent processes that separately contribute to the VEP delays along the visual pathways.

Considering the structure of the OR, using MRI parameters, Alshowaeir et al. have shown that in RRMS patients, dMRI parameters (MD and radial and axial diffusivities) along the OR are correlated with VEP latency (Alshowaeir et al., 2014). While MD is known to be a sensitive measure of white matter structure, as it has been correlated with age, learning, cognitive function, and disease states (Assaf and Pasternak, 2008; Horsfield and Jones, 2002; Zatorre et al., 2012; Yeatman et al., 2014), it is not specific, and can reflect changes in many tissue properties (myelin content, axonal orientation distribution, axon density etc.). Therefore, we hypothesized that using T1, which is mostly sensitive to water, myelin and iron content (Filo et al., 2019; Stüber et al., 2014), might be beneficial in predicting VEP latency. We found that in the OR of progressive MS patients, the T1 and MD values are in fact highly correlated, and produce similar results: when used as single parameters, MD outperformed T1, while when combined with the rest of the parameters in the PCA, T1 led to a slightly improved prediction of the VEP. It is therefore possible that in this case both MD and T1 represent the myelin damage. We also found that the RD is highly correlated with the MD, and consequently with the VEP latency as well. The FA and MTV, on the other hand, were not significantly correlated with the VEP latency, either because their estimation is noisier, or because they are less specific to the changes in myelin along the axons.

Our results suggest that if one has only a single measure in hand, using MD or RD along the OR is the best predictor of VEP latency, better than T1, pRNFL thickness, lesion load, and OR length. However,

when pairs of parameters are used, the combination of OR lesion load with either retinal thickness or MD gives the best prediction (supp. Fig. 10). This suggests that a lesion in the OR acts as a bottleneck and considerably delays the signal, and is therefore informative in predicting conduction delays, in particular when additional structural information of retinal thinning or dMRI is available.

It should be noted that the observed advantage of MD and T1 over the lesion load as single predictors, compared with the combination of the parameters which gives a better prediction when the lesion load is used, may be influenced by two participants. When combining the MD and the lesion load with the pRNFL thickness, in supplementary figure 10, we exclude two participants from the analysis, since they did not have pRNFL thickness estimates. The exclusion of these subjects increased the correlation of the VEP latency with the lesion load, but decreased its correlation with the MD. This opposite effect can account for the difference between the combined analysis (supp. Fig. 10), where the lesion load was more informative, and the single parameter analysis, where the lesion load was not informative.

Considering our results, we posit that the best approach was to perform PCA on the different structural sources (pRNFL thickness, OR lesion load, OR length, and OR microstructure). Using the 1st PC was better than the 6 other combination we tested, which include 5 pairwise combinations of the OR lesion load, the OR microstructure and the pRNFL thickness, as well as 1 combination of both OR microstructure measures (T1 and MD). The 1st PC was able to explain about 45% of the between-subject variance in VEP latency. Interestingly, using two correlated microstructural features (T1 and MD) in the PCA did not improve the VEP latency prediction. This highlights the contribution of other, non-microstructural measurements (pRNFL and OR lesion load), to the delay in VEP latency. The remaining variance can be explained given several other possible sources of inter-subject variability (supp. Fig. 3c shows, using repeated measurements, that no more than 66% of the variance can be explained). Such sources include retinal, thalamic and cortical processing times, as well as measurement noise. Conduction time is also influenced by the optic nerve and optic tract. However, the optic nerve is difficult to delineate, and optic tract analyses failed to produce any meaningful relationship (supp. Fig. 9). It is possible the variability in the reconstruction of the OR is another source of variability that may partly explain our results. Such tract variability could reflect changes in the underlying tissue caused by the disease. Nevertheless, heterogeneity in OR reconstruction can be seen in healthy subjects as well, particularly in Meyer's loop, due to the high curvature of the fibers passing through it (Sherbondy et al., 2008). While we cannot fully rule out some effects of differences in tractography, supplementary Fig. 11 shows that in this study, the individual variability in our estimates does not originate from the differences found in Meyer's loop reconstruction. Furthermore, additional analysis revealed these estimates can be used to predict the VEP latency even after excluding Meyer's loop.

VEP latency is most often used in the clinical setup in patients with ON and is thought to mainly reflect the conduction velocity along the optic nerve (Halliday et al., 1973), but our results suggest that the variance in the VEP latency can be explained using the properties of other parts of the visual system. Interestingly, in the subgroup of patients with a history of ON participating in our study, we could not find the same relationships between properties of the OR and the VEP latency as in patients without ON. Backner et al. showed that in patients with a history of ON, VEP latencies did not display an association with pRNFL thickness, but did display it with motion perception, a reflection of the functional deficits caused by the damage to the optic nerve (Backner et al., 2019). Such reflection of function was not seen in patients without ON, even with affected VEP latencies. This suggests that while in patients without ON, the structural properties of the OR may explain the observed delayed latencies, in ON patients, the structural integrity of the OR and its measurements have less weight and are not as relevant as the direct damage to the optic nerve.

It is important to note that the qMRI used in this study are sensitive, but not specific to tissue microstructure and properties. While T1 and MD each contribute to the prediction of VEP latency, their combination did not improve the prediction, neither when they were combined in a linear model (Fig. 4), nor when they were both included in the PCA. It is possible that with more advanced imaging acquisition and techniques we will be able to estimate tissue properties that are directly related to conduction such as myelin content, g-ratio, and axon diameter. A potential advantage of such parameterization is the ability to advance beyond the linear model we use here, and to estimate the conduction delay in a biophysical framework (Berman et al., 2019; Drakesmith et al., 2019). Nevertheless, it should be stressed that many of the existing models for calculating the tissue microstructure might be sub-optimal in pathological cases where the tissue undergoes many structural changes, and they may need to be accounted for in the future.

Our results further show that using the OR length in this patient group contributes little to the prediction of VEP latency. This does not suggest the OR length does not affect the VEP latency, but simply that in this study, predicting the VEP is better served by using the pRNFL, the MD/T1, and lesion load along the OR. The OR length was correlated with the VEP latency (after removing an outlier), therefore, it is possible that the lesions and axonal loss act as a bottleneck in the signal transmission, therefore delaying the VEP dramatically, and creating most of the variance between the subjects. With higher signal to noise measures and/or with a more complex, non-linear model, one might be able to account for the contribution of OR length and qMRI parameters to the variance in VEP latency.

Finally, while the OR lesion load contributed to the PCA, when used on its own it did not provide a good predictor for the VEP latency. In this study we used an automatic tool for lesion segmentation, and while it worked fairly well, it was not perfect. Furthermore, it might be beneficial to minimize registration errors between the lesion map and the diffusion data, by unwarping the diffusion data (Andersson et al., 2003). Nevertheless, our results suggest that the lesion load as the sole predictor of the damage to white matter structure should be used with caution.

In conclusion, in this study we predict the VEP latencies in a disease state using multiple structural sources along the visual pathway, with emphasis on the OR. Our results show the importance of combining those sources when attempting to show the connection between connectivity and conductivity. The visual system enables us to estimate both structural properties of its different elements, as well as a relatively direct estimate of its conduction properties, using VEPs. While the structure of many other systems in the brain can be evaluated with MRI, for many of them we cannot assess the conduction properties non-invasively, without electrical/magnetic stimulation. Therefore, establishing an understanding of the relationship between the structural properties and conduction in the visual system in multiple sclerosis is valuable to future studies of other brain systems and other white matter diseases.

Credit author statement

S.B. Conceptualization, analysis, and writing
Y.B Analysis of tractography, and writing
R.K. Implementation of lesion segmentation
F.P Analysis of OCT, reviewing manuscript
D.K Data curation, project administration
P.P Data curation, project administration
N.L Resources, supervision, reviewing and editing
A.M Conceptualization, supervision, reviewing and editing

Declaration of Competing Interest

None

Acknowledgments

We are grateful to all the patients and family members for their participation in this study. We thank Oshrat Shtangel for the helpful comments on the analysis.

Funding

This work was also supported by the National Multiple Sclerosis Society [Research Grant RG-1802-30165]; and the Applebaum Foundation. SB was supported by the Ministry of Science Technology & Space, Israel (Grant No. 3-13395). A.A.M was supported by the ISF Grant (No. 0399306) and the NSF/SBE-BSF Grants (NSF No. 1551330 and BSF No. 2015608). This work was also supported by a seed grant from the Eric Roland Fund for Interdisciplinary Research administered by ELSC, awarded to A.A.M. and S.B.. F.P. was supported by Deutsche Forschungsgemeinschaft (DFG Exc 257).

Supplementary materials

Supplementary material associated with this article can be found, in the online version, at doi:10.1016/j.neuroimage.2020.117204.

References

Alexander, A.L., Hurley, S.A., Samsonov, A.A., Adluru, N., Hosseinbor, A.P., Mossahebi, P., Field, A.S., 2011. Characterization of cerebral white matter properties using quantitative magnetic resonance imaging stains. Brain Connect.. http://doi.org/10.1089/brain.2011.0071.

Alshowaeir, D., Yiannikas, C., Garrick, R., Parratt, J., Barnett, M.H., Graham, S.L., Klistorner, A., 2014. Latency of multifocal visual evoked potentials in nonoptic neuritis eyes of multiple sclerosis patients associated with optic radiation lesions. Invest. Ophthalmol. Vis. Sci. 55 (6), 3758–3764. http://doi.org/10.1167/iovs.14-14571.

Andersson, J.L.R., Skare, S., Ashburner, J., 2003. How to correct susceptibility distortions in spin-echo echo-planar images: application to diffusion tensor imaging. Neuroimage 20 (2), 870–888. http://doi.org/10.1016/S1053-8119(03)00336-7.

Assaf, Y., Blumenfeld-Katzir, T., 2008. AxCaliber: a method for measuring axon diameter distribution from diffusion MRI. Magn. Reson. Med. Off. J. Int. Soc. Magn. Reson. Med. 59 (6), 1347–1354.

Assaf, Y., Pasternak, O., 2008. Diffusion Tensor Imaging (DTI)-based white matter mapping in brain research: a Review. J. Mol. Neurosci. 34 (1), 51–61. http://doi.org/10.1007/s12031-007-0029-0.

Avants, B., Tustison, N., Song, G., 2009. Advanced Normalization Tools (ANTS). Insight J. 1–35.

Backner, Y., Levin, N., 2018. Keep your eyes wide open: on visual- and vision-related measurements to better understand multiple sclerosis pathophysiology. J. Neuro-Ophthalmol. 38 (1), 85–90. http://doi.org/10.1097/WNO.0000000000000634.

Backner, Y., Petrou, P., Glick-Shames, H., Raz, N., Zimmermann, H., Jost, R., Levin, N., 2019. Vision and vision-related measures in progressive multiple sclerosis. Front. Neurol. 10. http://doi.org/10.3389/fneur.2019.00455.

Balcer, L.J., Miller, D.H., Reingold, S.C., Cohen, J.A., 2015. Vision and vision-related outcome measures in multiple sclerosis. Brain. Oxford University Press http://doi.org/10.1093/brain/awu335.

Barral, J.K., Gudmundson, E., Stikov, N., Etezadi-Amoli, M., Stoica, P., Nishimura, D.G., 2010. A robust methodology for in vivo T1 mapping. Magn. Reson. Med. 64 (4), 1057–1067. http://doi.org/10.1002/mrm.22497.

Basser, P.J., Jones, D.K., 2002. Diffusion-tensor MRI: theory, experimental design and data analysis - a technical review. NMR Biomed. 15 (7–8), 456–467. http://doi.org/10.1002/nbm.783.

Basser, P.J., Pajevic, S., Pierpaoli, C., Duda, J., Aldroubi, A., 2000. In vivo fiber tractography using DT-MRI data. Magn. Reson. Med. 44 (4), 625–632. http://doi.org/10.1002/1522-2594(200010)44:4<625::AID-MRM17>3.0.CO;2-O.

Berman, S., Filo, S., Mezer, A.A., 2019. Modeling conduction delays in the corpus callosum using MRI-measured g-ratio. Neuroimage 195, 128–139. http://doi.org/10.1016/j.neuroimage.2019.03.025.

Berman, S., West, K.L., Does, M.D., Yeatman, J.D., Mezer, A.A., 2018. Evaluating g-ratio weighted changes in the corpus callosum as a function of age and sex. Neuroimage 182, 304–313. http://doi.org/10.1016/j.neuroimage.2017.06.076.

Compston, A., Coles, A., 2008. Multiple sclerosis. Lancet. http://doi.org/10.1016/S0140-6736(08)61620-7.

Costello, F., 2016. Vision disturbances in multiple sclerosis. Semin. Neurol. 36 (2), 185–195. http://doi.org/10.1055/s-0036-1579692.

Dadar, M., Maranzano, J., Misquitta, K., Anor, C.J., Fonov, V.S., Tartaglia, M.C., Collins, D.L., 2017. Performance comparison of 10 different classification techniques in segmenting white matter hyperintensities in aging. Neuroimage 157, 233–249. http://doi.org/10.1016/j.neuroimage.2017.06.009.

Drakesmith, M., Harms, R., Rudrapatna, S.U., Parker, G.D., Evans, C.J., Jones, D.K., 2019. Estimating axon conduction velocity in vivo from microstructural MRI. Neuroimage 203. http://doi.org/10.1016/j.neuroimage.2019.116186.

Filo, S., Shtangel, O., Salamon, N., Kol, A., Weisinger, B., Shifman, S., Mezer, A.A., 2019. Disentangling molecular alterations from water-content changes in the aging human brain using quantitative MRI. Nat. Commun. 10 (1). http://doi.org/10.1038/s41467-019-11319-1.

Frohman, E., Costello, F., Zivadinov, R., Stuve, O., Conger, A., Winslow, H., Balcer, L., 2006. Optical coherence tomography in multiple sclerosis. Lancet Neurol.. http://doi.org/10.1016/S1474-4422(06)70573-7.

Galetta, S.L., Villoslada, P., Levin, N., Shindler, K., Ishikawa, H., Parr, E., Balcer, L.J., 2015. Acute optic neuritis: unmet clinical needs and model for new therapies. Neurol. Neuroimmunol. NeuroInflamm. 2 (4). http://doi.org/10.1212/NXI.0000000000000135.

Gregori, B., Pro, S., Bombelli, F., La Riccia, M., Accornero, N., 2006. Vep latency: sex and head size. Clin. Neurophysiol. 117 (5), 1154–1157. doi:10.1016/j.clinph.2006.01.014.

Halliday, A.M., McDonald, W.I., Mushin, J., 1973. Visual evoked response in diagnosis of multiple sclerosis. Br. Med. J. 4 (5893), 661–664. http://doi.org/10.1136/bmj.4.5893.661.

Helms, G., Dathe, H., Kallenberg, K., Dechent, P., 2008. High-resolution maps of magnetization transfer with inherent correction for RF inhomogeneity and T 1 relaxation obtained from 3D FLASH MRI. Magn. Reson. Med. 60 (6), 1396–1407. http://doi.org/10.1002/mrm.21732.

Horsfield, M.A., Jones, D.K., 2002. Applications of diffusion-weighted and diffusion tensor MRI to white matter diseases - a review. NMR Biomed. 15 (7–8), 570–577. http://doi.org/10.1002/nbm.787.

Kaden, E., Kelm, N.D., Carson, R.P., Does, M.D., Alexander, D.C., 2016. Multi-compartment microscopic diffusion imaging. Neuroimage 139, 346–359. http://doi.org/10.1016/j.neuroimage.2016.06.002.

Klistorner, A., Sriram, P., Vootakuru, N., Wang, C., Barnett, M.H., Garrick, R., Yiannikas, C., 2014. Axonal loss of retinal neurons in multiple sclerosis associated with optic radiation lesions. Neurology 82 (24), 2165–2172. http://doi.org/10.1212/WNL.0000000000000522.

Klistorner, A., Wang, C., Yiannikas, C., Parratt, J., Dwyer, M., Barton, J., Barnett, M.H., 2018. Evidence of progressive tissue loss in the core of chronic MS lesions: a longitudinal DTI study. NeuroImage: Clin. 17, 1028–1035. http://doi.org/10.1016/j.nicl.2017.12.010.

Kuchling, J., Backner, Y., Oertel, F.C., Raz, N., Bellmann-Strobl, J., Ruprecht, K., Scheel, M., 2018. Comparison of probabilistic tractography and tract-based spatial statistics for assessing optic radiation damage in patients with autoimmune inflammatory disorders of the central nervous system. Neuroimage Clin. 19, 538–550. http://doi.org/10.1016/j.nicl.2018.05.004.

Kuchling, J., Brandt, A.U., Paul, F., Scheel, M., 2017. Diffusion tensor imaging for multilevel assessment of the visual pathway: possibilities for personalized outcome prediction in autoimmune disorders of the central nervous system. EPMA J. 8 (3), 279–294. http://doi.org/10.1007/s13167-017-0102-x.

Langdon, D., Amato, M., Boringa, J., Brochet, B., Foley, F., Fredrikson, S., Benedict, R., 2012. Recommendations for a Brief International Cognitive Assessment for Multiple Sclerosis (BICAMS). Multiple Scler. J. 18 (6), 891–898. http://doi.org/10.1177/1352458511431076.

Meyers, S.M., Kolind, S.H., MacKay, A.L., 2017. Simultaneous measurement of total water content and myelin water fraction in brain at 3T using a T2 relaxation based method. Magn. Reson. Imaging 37, 187–194. http://doi.org/10.1016/j.mri.2016.12.001.

Mezer, A., Rokem, A., Berman, S., Hastie, T., Wandell, B.A., 2016. Evaluating quantitative proton-density-mapping methods. Hum Brain Mapp. 37 (10), 3623–3635. http://doi.org/10.1002/hbm.23264.

Mezer, A., Yeatman, J.D., Stikov, N., Kay, K.N., Cho, N.-J., Dougherty, R.F., Wandell, B.a., 2013. Quantifying the local tissue volume and composition in individual brains with magnetic resonance imaging. Nat. Med. 19 (12), 1667–1672. http://doi.org/10.1038/nm.3390.

Nitz, W.R., Reimer, P., 1999. Contrast mechanisms in MR imaging. Eur. Radiol.. http://doi.org/10.1007/s003300050789.

Oberwahrenbrock, T., Traber, G.L., Lukas, S., Gabilondo, I., Nolan, R., Songster, C., Schippling, S., 2018. Multicenter reliability of semiautomatic retinal layer segmentation using OCT. Neurol. Neuroimmunol. Neuroinflamm. 5 (3). e449 http://doi.org/10.1212/nxi.0000000000000449 .

Oertel, F.C., Zimmermann, H.G., Brandt, A.U., Paul, F., 2019. Novel uses of retinal imaging with optical coherence tomography in multiple sclerosis. Expert Rev. Neurother. 19 (1), 31–43. http://doi.org/10.1080/14737175.2019.1559051.

Pawlitzki, M., Neumann, J., Kaufmann, J., Heidel, J., Stadler, E., Sweeney-Reed, C., Schreiber, S., 2017. Loss of corticospinal tract integrity in early MS disease stages. Neurol. Neuroimmunol. Neuroinflamm. 4 (6). e399 http://doi.org/10.1212/NXI.0000000000000399 .

Petzold, A., Balcer, L., Calabresi, P.A., Costello, F., Frohman, T., Frohman, E., Zimmermann, H., 2017. Retinal layer segmentation in multiple sclerosis: a systematic review and meta-analysis. Lancet Neurol. 16 (10), 797–812. http://doi.org/10.1016/S1474-4422(17)30278-8.

Polman, C.H., Reingold, S.C., Banwell, B., Clanet, M., Cohen, J.A., Filippi, M., Wolinsky, J.S., 2011. Diagnostic criteria for multiple sclerosis: 2010 Revisions to the McDonald criteria. Ann. Neurol. 69 (2), 292–302. http://doi.org/10.1002/ana.22366.

Raz, N., Bick, A.S., Ben-Hur, T., Levin, N., 2015. Focal demyelinative damage and neighboring white matter integrity: an optic neuritis study. Mult. Scler. 21 (5), 562–571. http://doi.org/10.1177/1352458514551452.

Raz, N., Chokron, S., Ben-Hur, T., Levin, N., 2013. Temporal reorganization to overcome monocular demyelination. Neurology 81 (8), 702–709. http://doi.org/10.1212/WNL.0b013e3182a1aa3e.

Raz, N., Dotan, S., Benoliel, T., Chokron, S., Ben-Hur, T., Levin, N., 2011. Sustained motion perception deficit following optic neuritis: behavioral and cortical evidence. Neurology 76 (24), 2103–2111. http://doi.org/10.1212/WNL.0b013e31821f4602.

Reese, T.G., Heid, O., Weisskoff, R.M., Wedeen, V.J., 2003. Reduction of eddy-current-induced distortion in diffusion MRI using a twice-refocused spin echo. Magn Reson Med 49 (1), 177–182. http://doi.org/10.1002/mrm.10308.

Sanders, E.A.C.M., Volkers, A.C.W., Van der Poel, J.C., Van Lith, G.H.M., 1987. Visual function and pattern visual evoked response in optic neuritis. Br. J. Ophthalmol. 71 (8), 602–608. http://doi.org/10.1136/bjo.71.8.602.

Schippling, S., Balk, L.J., Costello, F., Albrecht, P., Balcer, L., Calabresi, P.A., Petzold, A., 2015. Quality control for retinal OCT in multiple sclerosis: validation of the OSCAR-IB criteria. Mult. Scler. 21 (2), 163–170. http://doi.org/10.1177/1352458514538110.

Schurr, R., Duan, Y., Norcia, A.M., Ogawa, S., Yeatman, J.D., Mezer, A.A., 2018. Tractography optimization using quantitative T1 mapping in the human optic radiation. Neuroimage 181, 645–658. doi:10.1016/j.neuroimage.2018.06.060.

Sherbondy, A.J., Dougherty, R.F., Napel, S., Wandell, B.A., 2008. Identifying the human optic radiation using diffusion imaging and fiber tractography. J Vis 8 (10). http://doi.org/10.1167/8.10.12.

Sinnecker, T., Oberwahrenbrock, T., Metz, I., Zimmermann, H., Pfueller, C.F., Harms, L., Wuerfel, J., 2015. Optic radiation damage in multiple sclerosis is associated with visual dysfunction and retinal thinning – an ultrahigh-field MR pilot study. Eur. Radiol. 25 (1), 122–131. http://doi.org/10.1007/s00330-014-3358-8.

Sled, J.G., Pike, G.B., 2001. Quantitative imaging of magnetization transfer exchange and relaxation properties in vivo using MRI. Magn. Reson. Med. 46 (5), 923–931. http://doi.org/10.1002/mrm.1278.

Sriram, P., Wang, C., Yiannikas, C., Garrick, R., Barnett, M., Parratt, J., Klistorner, A., 2014. Relationship between optical coherence tomography and electrophysiology of the visual pathway in non-optic neuritis eyes of multiple sclerosis patients. PLoS ONE 9 (8), e102546. http://doi.org/10.1371/journal.pone.0102546.

Stikov, N., Perry, M.L., Mezer, A., Rykhlevskaia, E., Wandell, B.a., Pauly, john m., Dougherty, R.F., 2012. Bound pool fractions complement diffusion measures to describe white matter micro and macrostructure. Neuroimage 29 (6), 997–1003. http://doi.org/10.1016/j.biotechadv.2011.08.021.Secreted.

Stüber, C., Morawski, M., Schäfer, A., Labadie, C., Wähnert, M., Leuze, C., Turner, R., 2014. Myelin and iron concentration in the human brain: a quantitative study of MRI contrast. Neuroimage 93 (P1), 95–106. http://doi.org/10.1016/j.neuroimage.2014.02.026.

Takemura, H., Yuasa, K., Amano, K., 2020. Predicting neural response latency of the human early visual cortex from MRI-based tissue measurements of the optic radiation. eNeuro ISO 690.

Talman, L.S., Bisker, E.R., Sackel, D.J., Long, D.A., Galetta, K.M., Ratchford, J.N., Balcer, L.J., 2010. Longitudinal study of vision and retinal nerve fiber layer thickness in MS. Ann. Neurol.. NA-NA http://doi.org/10.1002/ana.22005 .

Toosy, A.T., Mason, D.F., Miller, D.H., 2014, January. Optic neuritis. Lancet Neurol.. http://doi.org/10.1016/S1474-4422(13)70259-X.

Weiskopf, N., Mohammadi, S., Lutti, A., Callaghan, M.F., 2015. Advances in MRI-based computational neuroanatomy. Curr. Opin. Neurol. 28 (4), 313–322. http://doi.org/10.1097/WCO.0000000000000222.

Yeatman, J.D., Dougherty, R.F., Myall, N.J., Wandell, B.a., Feldman, H.M., 2012. Tract profiles of white matter properties: automating fiber-tract quantification. PLoS ONE 7 (11). http://doi.org/10.1371/journal.pone.0049790.

Yeatman, J.D., Wandell, B.A., Mezer, A.A., 2014. Lifespan maturation and degeneration of human brain white matter. Nat. Commun. 5, 4932. doi:10.1038/ncomms5932.

Zatorre, R.J., Fields, R.D., Johansen-Berg, H., 2012. Plasticity in gray and white: neuroimaging changes in brain structure during learning. Nat. Neurosci. 15 (4), 528–536. http://doi.org/10.1038/nn.3045.

Zhang, H., Schneider, T., Wheeler-Kingshott, C.a., Alexander, D.C., 2012. NODDI: practical in vivo neurite orientation dispersion and density imaging of the human brain. Neuroimage 61 (4), 1000–1016. http://doi.org/10.1016/j.neuroimage.2012.03.072</bib.